JGR Space Physics

RESEARCH ARTICLE
10.1029/2024JA032905

On the Contribution of Latitude-Dependent ULF Waves to the Radial Transport of Off-Equatorial Relativistic Electrons in the Radiation Belts

Theodore E. Sarris[1,2], Xinlin Li[2,3], Hong Zhao[4], Weichao Tu[5], Kostis Papadakis[6], Stelios Tourgaidis[1], Wenlong Liu[7], Li Yan[7], Robert Rankin[8], Zheng Xiang[2], Yang Mei[2,3], Declan O'Brien[2,3], Benjamin Hogan[2,3], David Brennan[2], Robert E. Ergun[2], Vassilis Angelopoulos[9], Dimitris Baloukidis[1], and Panagiotis Pirnaris[1]

[1]Department of Electrical Engineering, Democritus University of Thrace, Xanthi, Greece, [2]Laboratory for Atmospheric & Space Physics, University of Colorado Boulder, Boulder, CO, USA, [3]Department of Aerospace Engineering Sciences, University of Colorado Boulder, Boulder, CO, USA, [4]Department of Physics, Auburn University, Auburn, AL, USA, [5]Department of Physics and Astronomy, West Virginia University, Morgantown, WV, USA, [6]Department of Physics, University of Helsinki, Helsinki, Finland, [7]School of Space and Earth Sciences, Beihang University, Beijing, China, [8]University of Alberta, Edmonton, AB, Canada, [9]University of California at Los Angeles, Los Angeles, CA, USA

Key Points:

- Enhanced Ultra-low frequency (ULF) wave power at high latitudes significantly enhances radial transport of off-equatorial relativistic radiation belt electrons
- Radial diffusion coefficients need to be revisited, to include pitch angle dependence and latitude-dependent ULF wave power
- These results are enabled by multi-year statistics by s/c performing measurements away from the magnetic equator and by particle tracing

Correspondence to:
T. E. Sarris,
tsarris@ee.duth.gr

Citation:
Sarris, T. E., Li, X., Zhao, H., Tu, W., Papadakis, K., Tourgaidis, S., et al. (2024). On the contribution of latitude-dependent ULF waves to the radial transport of off-equatorial relativistic electrons in the radiation belts. *Journal of Geophysical Research: Space Physics*, *129*, e2024JA032905. https://doi.org/10.1029/2024JA032905

Received 23 MAY 2024
Accepted 11 OCT 2024

Author Contributions:
Conceptualization: Theodore E. Sarris
Data curation: Theodore E. Sarris, Xinlin Li, Wenlong Liu, Li Yan, Robert E. Ergun, Vassilis Angelopoulos
Formal analysis: Theodore E. Sarris, Hong Zhao, Weichao Tu
Funding acquisition: Theodore E. Sarris, Xinlin Li, Robert E. Ergun, Vassilis Angelopoulos
Investigation: Theodore E. Sarris, Xinlin Li, Hong Zhao, Weichao Tu, Zheng Xiang, Yang Mei, Declan O'Brien, Benjamin Hogan, David Brennan, Dimitris Baloukidis, Panagiotis Pirnaris
Methodology: Theodore E. Sarris, Hong Zhao, Weichao Tu, Kostis Papadakis, Stelios Tourgaidis, Wenlong Liu, Yang Mei

Abstract Ultra-low frequency (ULF) waves radially diffuse hundreds-keV to few-MeV electrons in the magnetosphere, as the range of drift frequencies of such electrons overlaps with the wave frequencies, leading to resonant interactions. Theoretically this process is described by analytic expressions of the resonant interactions between electrons and ULF wave modes in a background magnetic field. However, most expressions of the radial diffusion rates are derived for equatorially mirroring electrons and are based on estimates of the power of ULF waves that are obtained either from spacecraft close to the equatorial plane or from the ground but mapped to the equatorial plane. Based on recent statistical in situ observations, it was found that the wave power of magnetic fluctuations is significantly enhanced away from the magnetic equator. In this study, the distribution of the wave amplitudes as a function of magnetic latitude is compared against models simulating the natural modes of oscillation of magnetospheric field lines, with which they are found to be consistent. Energetic electrons are subsequently traced in 3D model fields that include a latitudinal dependence that is similar to measurements and to the natural modes of oscillation. Particle tracing simulations show a significant dependence of the radial transport of relativistic electrons on pitch angle, with off-equatorial electrons experiencing considerably higher radial transport, as they interact with ULF wave fluctuations of higher amplitude than equatorial electrons. These findings point to the need for incorporating pitch-angle-dependent radial diffusion coefficients in global radiation belt models.

Plain Language Summary The random inward and outward motion of high energy electrons in the Earth's magnetosphere, called radial diffusion, is a critical factor in modeling and predicting the state of the radiation belts, where many satellites operate. This motion is caused primarily by waves in the Ultra-Low Frequency (or ULF) range, which have been measured and characterized since the early days of the space era. However, for simplicity, most current models treat radial diffusion in two dimensions, on the Earth's magnetic equatorial plane, taking into account the average motion of electrons as they drift around the Earth. Recent studies, enabled by multi-year measurements by missions with off-equatorial inclinations (THEMIS, Arase, Cluster) have shown that the power of ULF waves is significantly enhanced away from the magnetic equator. A 3D model of the magnetic field fluctuations is compared with statistical data of the measured ULF wave power, and is then used to estimate the radial transport of off-equatorial electrons. It is found through single-particle tracing that radial diffusion is significantly enhanced when taking into account the latitude-dependence of ULF waves. These new findings can change the quantification and parameterization of radial diffusion and our current understanding of radial diffusion in the radiation belts.

1. Introduction

Almost simultaneously with the beginning of the space era and the discovery of the Earth's radiation belts, the concept of radial diffusion was proposed as a key acceleration mechanism responsible for the formation of the radiation belts. However, despite more than 60 years of research, the effectiveness and quantification of radial

Project administration: Theodore E. Sarris
Resources: Theodore E. Sarris, Xinlin Li
Software: Theodore E. Sarris, Kostis Papadakis, Stelios Tourgaidis, Robert Rankin, Dimitris Baloukidis, Panagiotis Pirnaris
Supervision: Theodore E. Sarris
Validation: Theodore E. Sarris, Xinlin Li, Hong Zhao, Weichao Tu, Kostis Papadakis, Stelios Tourgaidis, Wenlong Liu, Robert Rankin, Zheng Xiang
Visualization: Theodore E. Sarris, Zheng Xiang, Dimitris Baloukidis, Panagiotis Pirnaris
Writing – original draft: Theodore E. Sarris
Writing – review & editing: Theodore E. Sarris, Xinlin Li, Hong Zhao, Weichao Tu, Zheng Xiang, Yang Mei, Declan O'Brien, Benjamin Hogan, David Brennan

diffusion and aspects of the underlying theory are still subjects of active research and debate. A cornerstone in analytically describing the process of drift-resonant radial diffusion is the work by Fälthammar (1965, 1968), who used simplified expressions for electric and magnetic fluctuations to derive diffusion coefficients. In these early studies, due to a lack of in situ observations, expressions for radial diffusion have been derived assuming impulsive variations of the geomagnetic field and a corresponding induced electric field (Parker, 1960), thus focusing primarily on the diffusive effects of compressional perturbations of the background magnetic field. Various studies over the years since this monumental work have explored the validity of the main assumptions of the diffusion coefficients introduced by Fälthammar (1965), expanding and re-deriving their proposed analytic expressions and/or emphasizing the effects of the asymmetries in the Earth's magnetic field, the resonant interactions of poloidal and toroidal waves, and other. Based on these studies, various models have been proposed that use parametric approximations of the power spectral densities of magnetic field oscillations and electric field oscillations in the Pc4 and Pc5 ranges of frequencies (6.7–22.2 mHz and 1.7–6.7 mHz, respectively; see Jacobs et al., 1964), which subsequently feed into theoretical approximations of the diffusion coefficients of radial transport, or D_{LL}, of energetic particles. Examples include the parameterizations by Selesnick et al. (1997), Brautigam and Albert (2000), Elkington et al. (2003), Brautigam et al. (2005), Perry et al. (2005), Barker et al. (2005), Fei et al. (2006), Sarris et al. (2006), Huang et al. (2010), Tu et al. (2012), Rae et al. (2012), Lejosne et al. (2013), Ozeke et al. (2014), Dimitrakoudis et al. (2015), Ali et al. (2015, 2016), Liu et al. (2016), Cunningham (2016), Barani et al. (2019), Olifer et al. (2019), Katsavrias et al. (2022), and others. With the exception of the model by Cunningham (2016) that is further discussed below, all the aforementioned models provide radial diffusion coefficients that are limited to near-equatorially trapped electrons that interact with electric and magnetic field perturbations that are measured or that are assumed to occur close to the equatorial plane.

Due to the assumptions that are made and the data that are used in the above studies, there is one key aspect that has not been investigated at great length: the pitch-angle dependence of the diffusion coefficients and the applicability of existing diffusion coefficients for off-equatorial particles, under realistic, 3D wave power distributions. It is noted that the diffusive effects of drift shell splitting in a distorted magnetic field and the resulting so-called anomalous radial diffusion caused by elastic pitch angle scattering have been investigated theoretically early on (e.g., Fälthammar & Walt, 1969; Schulz & Lanzerotti, 1974, Sections III.7 and III.8 A), as well as revisited recently in a critical evaluation (Zheng et al., 2016). Furthermore, Li, Zhou, et al. (2021); Li, Liu, et al. (2021) have studied the bifurcations of particles' orbits because of off-equatorial magnetic field minima. In another study, Cunningham (2016) investigated the effects of compressional ULF perturbations on off-equatorial electrons in empirical, non-symmetric 3D background fields on top of which they added model ULF perturbations and explored the deviation of radial diffusion coefficients compared to the case of symmetric, dipole fields. They found that the new diffusion coefficients are substantially larger than those computed with a dipole background field model for equatorially mirroring particles. However, similarly to earlier studies, they also used simplifying models for their analytic perturbations, which are based on impulsive variations, rather than realistic measurements of the 3D distribution of ULF waves in L, azimuth, and magnetic latitude.

This work is motivated by a recent study of Sarris et al. (2022), in which the statistical distribution of ULF wave power in magnetic field fluctuations was quantified as a function of magnetic latitude. This was enabled by the inclinations of the orbits of the THEMIS and Arase missions, which are, on average, 11° and 31° respectively, and which, taking into account the Earth's dipole tilt, allow sampling magnetic latitudes up to ∼42.5°. The statistical analyses of that study showed that the transverse components of ULF wave power are significantly enhanced away from the magnetic equator, by more than an order of magnitude. These results were enabled by extended, multi-year statistics that are now available from these two missions. The results of the study by Sarris et al. (2022) have since been further confirmed by multi-year statistical analyses by Yan et al. (2023) that was based on measurements from the Cluster four-spacecraft mission, the inclinations of which allow sampling magnetic latitudes up to ∼50°. The effects of such enhanced ULF wave power away from the magnetic equator on energetic particles in the radiation belts have never been explored, as current formulations of the diffusion coefficients do not include a pitch angle dependence. Considering that non-equatorial particles traveling along a bounce-motion trajectory will spend most of their time near the mirror points, it can be anticipated that the effects of the enhanced off-equatorial ULF wave power on the radial diffusion and transport of electrons will be significant.

In view of the current lack of analytic derivations of a pitch-angle-dependent diffusion coefficient, particle tracing provides a means to accurately investigate the effects of electric and magnetic field fluctuations in diffusing and radially transporting energetic electrons. Particle tracing also enables extracting analytically parameterized

formulations of diffusion coefficients, as has been demonstrated for 1D (L-dependent) diffusion coefficients in Sarris et al. (2006) via 2D guiding center simulations. In this work, 3D guiding center particle tracing simulations are performed for electrons under model electric and magnetic field fluctuations with a 3D analytic formulation that includes a latitudinal dependence. The electrons' L is monitored in time over several drift periods under the effect of the ULF waves, and radial diffusion coefficients are derived from the electrons' average squared displacement in L over time, similarly to the methodology employed by Sarris et al. (2006). For the model 3D ULF waves, analytic expressions are constructed for the electric and magnetic field perturbations that are based on a comparison of the statistical measurements of the magnetic field perturbations with the natural modes of vibration for the magnetic field lines when they are resonantly excited by external driver signals. The comparisons, as presented herein, indicate that the amplitudes and latitudinal dependence of the model field fluctuations are in reasonably good agreement with the statistical measurements of broadband ULF waves in the frequencies of interest.

In the following, we first present in situ satellite measurements of the statistical distribution in magnetic latitude of the ULF wave power in the radial component of the magnetic field; these are used to guide the particle tracing simulations that are performed herein. Subsequently, we introduce the analytic model field formulations that are used in the particle tracing simulations and their comparison with statistical measurements. Next, the particle tracing simulation results are presented, with emphasis on the calculation of the local diffusion coefficient and its pitch angle dependence. Finally, we discuss potential implications of these simulation results on the current understanding of radial transport of electrons in the radiation belts. In view of the enhanced off-equatorial radial diffusion that is estimated through the simulations, specific mentions are made on the importance of introducing a pitch angle dependence in novel expressions of the diffusion coefficients, and on the implications for the quantification of electrostatic versus electromagnetic diffusion and their relative importance.

2. Statistical Distribution of ULF Waves in Magnetic Latitude

As discussed above, current analytic expressions for the radial diffusion coefficients require knowledge of the wave power of ULF waves as a function of L and wave frequency. This knowledge of ULF waves most commonly comes either from spacecraft close to the equatorial plane or from ground measurements, and thus refers to the waves' properties at the equatorial plane. In a recent study, Sarris et al. (2022) used measurements from the THEMIS and Arase missions and presented a statistical analysis of the distribution of ULF magnetic field wave power in magnetic latitude and local time. This study was enabled by the inclinations of the spacecraft orbits, which, together with the Earth's dipole tilt, allow sampling magnetic latitudes up to ∼42.5°, and up to ∼40° with statistical significance. Using 3.5 years of measurements from the two missions, Sarris et al. (2022) have shown that wave power of the transverse magnetic field components of ULF fluctuations increase away from the magnetic equator, with the radial component increasing by more than an order of magnitude. In terms of local time, the statistical analysis has shown that wave power is lower in the dayside than in the nightside at $L = 5$ to 9. The azimuthal component was found to have similar distributions, albeit with smaller power than the radial component, whereas the parallel component was found to be the weakest among the three, with more wave power concentrated around the magnetic equator. These results have recently been confirmed by Yan et al. (2023), who used 19 years of measurements from the Cluster four-spacecraft mission (Escoubet et al., 1997): the 90° inclination of the Cluster spacecraft allows the sampling of ULF waves from −50° to 50° in MLAT, extending the latitudes that can be sampled by THEMIS and Arase, as presented in Sarris et al. (2022).

In Sarris et al. (2022), the power of ULF waves was calculated for frequencies from 1.7 to 22.2 mHz, spanning the Pc4 and Pc5 frequency ranges (Jacobs et al., 1964), whereas in Yan et al. (2023) the power of ULF waves was calculated from 1.7 to 6.7 mHz, corresponding to the Pc5 frequency range. To simulate the drift-resonant interactions of electrons of a fixed energy or first adiabatic invariant μ with the ULF waves, the amplitude of the waves needs to be known for the drift frequency of the traced particles. In the following, the radial transport rates are calculated for electrons of a fixed first adiabatic invariant of $\mu = 1{,}000$ MeV/G, under their interaction with random broadband fluctuations, over several electron drift periods; assuming a range of L from 3 to 8 for the simulations and a range of pitch angles from 20° to 90°, the corresponding drift frequencies, calculated according to Roederer and Zhang (2014), are found to be in the range from 0.5 to 2 mHz for the electrons with $\mu = 1{,}000$ MeV/G. In comparison, it is noted that the ULF range of frequencies in the studies of both Sarris et al. (2022) and Yan et al. (2023) fail to cover the lower end of drift frequencies of the electrons of interest of this study. Thus, to estimate the amplitudes of the waves that will resonantly interact with the electrons of interest, the

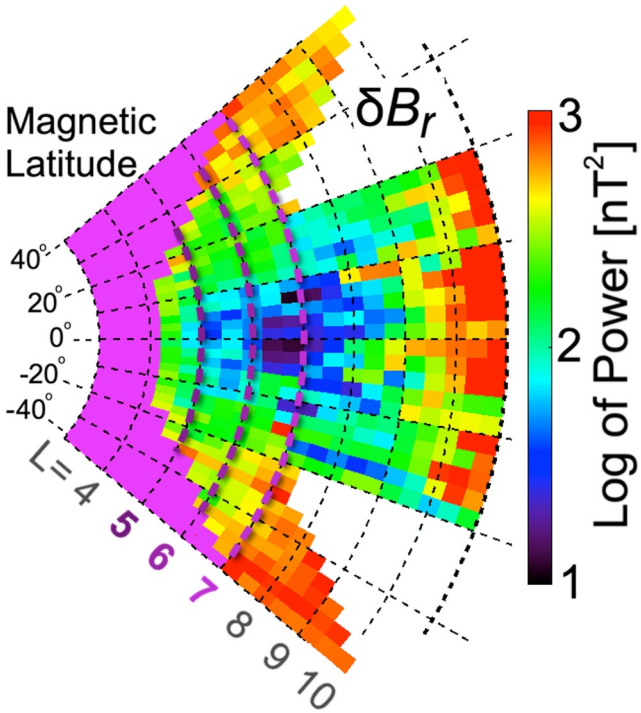

Figure 1. Distribution of the average integrated power as a function of L and magnetic latitude based on 3.5 years of THEMIS and Arase measurements, for the radial components of the magnetic field, δB_r, integrated over frequencies from 0.5 to 2.0 mHz. Areas of artificially enhanced wave power due to high spacecraft velocity are color-masked in magenta.

THEMIS & Arase data of Sarris et al. (2022) and the Cluster data of Yan et al. (2023) are re-processed by integrating the power spectral density over frequency from 0.5 to 2 mHz, to obtain the average squared amplitude over the frequencies of interest. The integration is done according to:

$$\delta B_r^2 = \int_{f_1}^{f_2} \mathrm{PSD}_B(f)\, df$$

where δB_r^2, expressed in units of nT^2, is the mean of the squared amplitude of the fluctuations in the magnetic field radial component, corresponding to the mean integrated power over the frequency range of interest, PSD_B is the power spectral density of the radial component of the magnetic field fluctuations, which is expressed in units of nT^2/Hz, and f_1 and f_2 are, respectively, the lower and upper limits of the frequencies of interest, which are set here to 0.5 and 2 mHz respectively. Similarly to Sarris et al. (2022), PSD_B is calculated using a wavelet transform with a Morlet mother wavelet, based on the methodology described in Torrence and Compo (1998). The resulting amplitudes of the waves are averaged, in log scale, over the time period of observation by the Arase and THEMIS spacecraft, and are normalized according to the total observation time per bin.

The results of the statistical distribution of ULF wave in magnetic latitude are presented in Figure 1, where the distribution of integrated wave power of the radial component of the magnetic field fluctuations is plotted in logarithmic scale. The calculation of wave power follows the same processing steps as the ones described in Sarris et al. (2022), the only difference being the new frequency range that is considered herein. In comparing the results of Figure 1 with the results of Figure 3 of Sarris et al. (2022), the distribution in latitude of the ULF wave power in the two figures are similar, in that they both reveal a pronounced minimum in the wave power of the radial component of broadband ULF waves at the magnetic equator; however an enhancement by approximately one order of magnitude can be observed in the wave power for the frequency range from 0.5 to 2 mHz compared to the frequency range from 1.7 to 22 mHz that was used in Sarris et al. (2022). In Figure 1, $L = 5$, 6, and 7 are marked as dashed lines in dark purple, purple, and light purple, respectively; these are the locations in L where particles are traced in the following. Similarly to the study of Sarris et al. (2022), the regions where the spacecraft velocity is too high to be able to resolve ULF wave power is masked in magenta. The average amplitude of the ULF waves that is shown in Figure 1, as it has been re-calculated based on the analysis of Sarris et al. (2022) for the frequencies of interest from 0.5 to 2 mHz, is used in the following to inform the estimation of the amplitudes of the model fields in the particle tracing simulation.

3. Analytic Model of Perturbation Fields

The perturbation fields are introduced in the particle tracing simulations through latitude-dependent, 3D analytic functions of ULF magnetic field wave amplitudes. These analytic expressions are formulated based on an observed similarity between the statistical results of the magnetic field wave amplitudes, as shown in Figure 1, and the modeled latitude dependence of the natural modes of poloidal oscillation of magnetic and electric field in the magnetosphere, as described in, for example, Wang et al. (2018), Degeling et al. (2019), Li, Liu, et al. (2021) and Li, Zhou, et al. (2021). The poloidal ULF waves are characterized by magnetic field oscillations in the radial component and electric field oscillations in the azimuthal component. It is noted that, in the analytic model that is used in this study, field perturbations of the compressional component are not considered. Furthermore, the transition between poloidal and toroidal waves is not considered. It is also noted, however, that the poloidal mode is expected to have dominant effects compared to the toroidal mode; this is further discussed in the discussions section. The latitudinal dependence of the model poloidal oscillation amplitudes is shown in Figures 2b and 2d, plotted in thick red and blue lines for the radial magnetic and azimuthal electric fields respectively. In this model, the natural modes of oscillation are derived via MHD (magnetohydrodynamic) simulations of the natural modes of vibration for the magnetic field lines, which are resonantly excited by an imposed driver signal, provided there

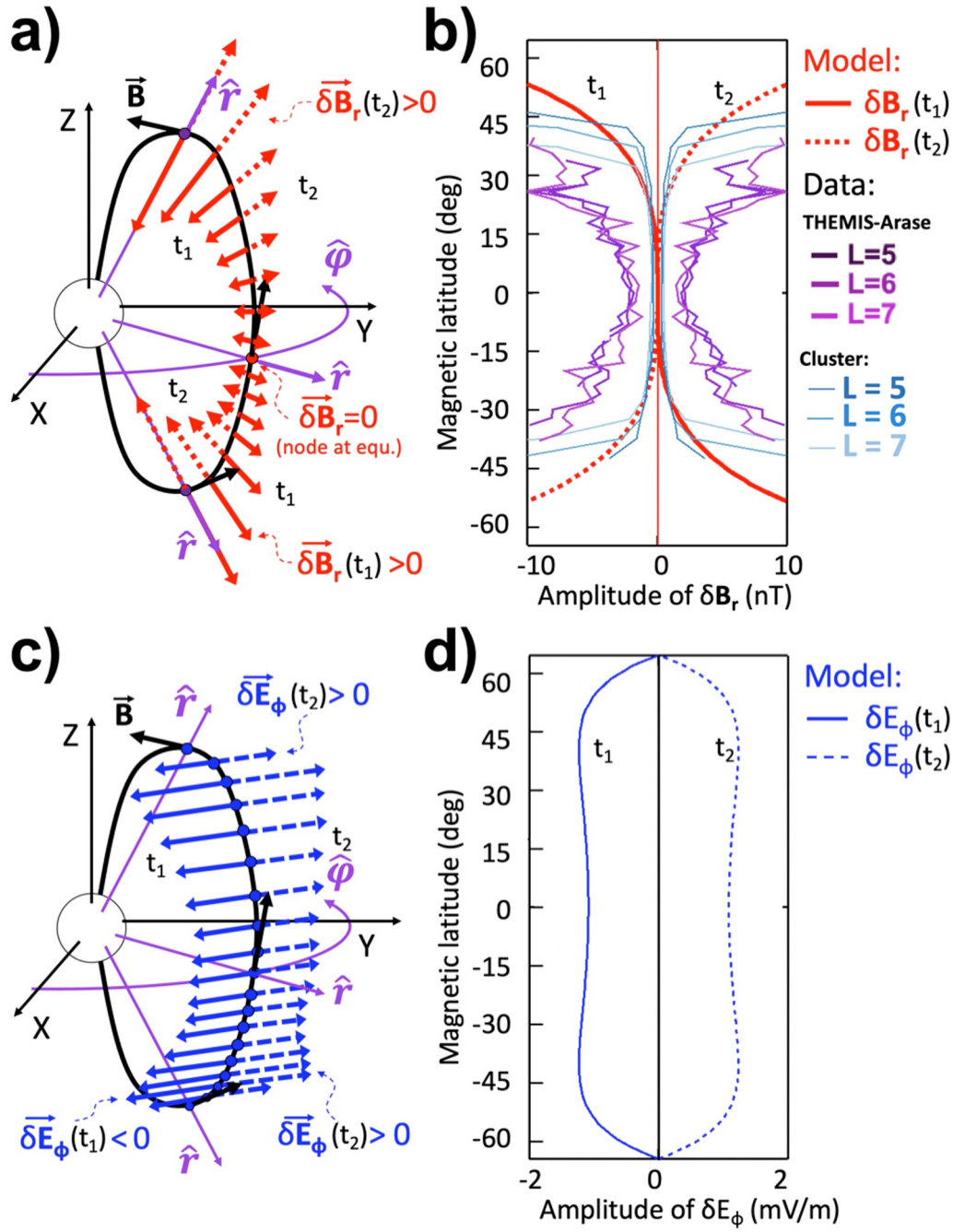

Figure 2. (a) Magnetic field oscillations of the radial component of the fundamental poloidal mode, for snapshots t_1 and t_2 corresponding to phases 0° (solid red vectors) and 180° (dashed red vectors) in the oscillation of a field line. (b) Amplitude of the radial component of the fundamental poloidal mode as a function of latitude, according to the model described in Degeling et al. (2019), for snapshots t_1 and t_2 corresponding to phases 0° (solid red line) and 180° (dashed red line). Overplotted are measurements of amplitudes from THEMIS and Arase as a function of latitude, at $L = 5$, 6, and 7 (dark purple, purple, and light purple lines, respectively), and from Cluster, also at $L = 5$, 6, and 7, obtained from Yan et al. (2023) (dark blue, blue, and light blue lines, respectively). (c) Same as (a), but for the vectors of the model azimuthal electric field oscillations. (d) Same as (b), but for the amplitudes of the model azimuthal electric field oscillations.

is nonzero spectral power in the driver at the local eigenfrequency. In Figure 1 of Li, Zhou, et al. (2021), Li, Liu, et al. (2021), which shows a schematic representation of the temporal evolution of ULF waves within one complete wave cycle of the poloidal waves at and off the magnetic equator using a wave model based on Wang

et al. (2018), a rapid enhancement can be seen as a function of magnetic latitude away from the equatorial plane for the radial component of magnetic field fluctuations, while a node exists at the equatorial plane. Furthermore, the northern and southern hemispheres are in different phases around the equatorial node; a similar phase difference is introduced in the model fields used herein.

The analytic functions that are used herein to capture this latitude dependence of the amplitude are given below in Equations 1 and 2 for the radial magnetic and the azimuthal electric field oscillations, respectively. In these equations, the first term colored in purple is the amplitude that is introduced to best match the model by Li, Liu, et al. (2021), Li, Zhou, et al. (2021), supported by the observations of the magnetic field fluctuations that are shown in Figure 1. The second term colored in green introduces an azimuthal modulation for the ULF wave fluctuations as a function of local time, or azimuth, φ, which takes the form of a dayside-nightside asymmetry. Thus, in the following simulations, ULF perturbations are considered to be of mode number $m = 1$. This assumption is consistent with the results by Elkington et al. (2012), who used simulation results from the Lyon-Fedder-Mobarry (LFM) MHD model (Lyon et al., 2004), and showed that azimuthal wave number $m = 1$ usually dominates, with the power spectral density of ULF waves usually residing in mode numbers $m < 3$. This is also consistent with the results from Sarris (2014), who presented a novel technique to extract the power per mode number from geosynchronous data, and also Sarris and Li (2017), who showed that, in the dayside region, power is distributed mostly to the lowest azimuthal wave numbers, $m = 1$ and 2. It is noted that, as indicated in Sarris (2014), Sarris and Li (2017), and Barani et al. (2019), higher modes might be more important during active times and in the Earth's magnetotail; simulating the effects of off-equatorial ULF waves during different geomagnetic conditions and in an asymmetric magnetosphere is beyond the scope of this study. The third term that is marked in black includes the temporal dependence of the ULF oscillations, where ω is the frequency of the ULF oscillation and t represents time. It is noted that in the electric field perturbation term a phase difference of $\pi/2$ is introduced between the magnetic and electric field perturbations. This is consistent with the findings of, for example, Singer et al. (1982), who reported that Alfvénic standing waves in the magnetosphere are characterized by a $\pi/2$ phase difference between the electric field and magnetic field components. As discussed in many subsequent studies, the sign of the phase delay is related to the harmonic mode of the ULF waves; for poloidal mode fundamental waves that are considered herein, the phase of the azimuthal electric field, δE_{φ}, leads the phase of the radial magnetic field perturbations, δB_r, by $\pi/2$ (e.g., Hao et al., 2017; Liu et al., 2013; Takahashi et al., 2011; Zhang et al., 2018, 2019). The last term, colored in red for the magnetic field and in blue for the electric field, introduces the latitude dependence of the ULF oscillation, and is set to match the modeled magnetic and electric fluctuations, respectively. For reconstructing broad-band fluctuations, the sum of 20 individual frequency components is used, as done, for example, in Sarris et al. (2006, 2017). These are randomly selected in the range from 0.5 to 2.0 mHz. Random phases are used for each component, and each particle trace run uses different randomizations. The individual amplitudes are set so that the sum of all amplitudes compares well against the amplitudes of the model MHD fluctuations according to Wang et al. (2018), Degeling et al. (2019), Li, Liu, et al. (2021), and Li, Zhou, et al. (2021), as discussed below.

$$\delta B_r = B_{0\_r}\ 0.5\,[1+\cos(\phi)]\ \sin(\omega t)\ \tan(0.6\,\lambda)^3 \quad (1)$$

amplitude | azimuthal modulation | temporal variation | latitudinal dependence

$$\delta E_{\varphi} = E_{0\_\varphi}\ 0.5\,[1+\cos(\phi)]\ \sin(\omega t + \pi/2)\ \left[e^{-[(\lambda+60^{\circ})/25^{\circ}]^2/2} + e^{-[(\lambda-60^{\circ})/25^{\circ}]^2/2}\right] \quad (2)$$

amplitude | azimuthal modulation | temporal variation | latitudinal dependence

In Figure 2 we plot a schematic representation of the latitudinal dependence of the above formulations, as follows: Figure 2a shows the vectors of the radial component of magnetic field oscillations δB_r for the fundamental poloidal mode. Two snapshots are plotted: one snapshot corresponding to a phase of 0° in the oscillation of a field line, which is marked as time t_1 and is plotted with solid vectors, and one snapshot corresponding to a phase of

180°, which is marked as t_2 and is plotted with dashed vectors. As can be seen in this panel, there is a node for δB_r at the magnetic equator for the fundamental poloidal mode, and a reversal in polarity between the northern and southern hemispheres. Figure 2b shows the corresponding amplitude of δB_r as a function of latitude, according to the model described in Degeling et al. (2019), for the same two snapshots shown in Figure 2a: the snapshot corresponding to a phase of 0° is plotted with a thick solid red line and is marked as t_1 whereas the snapshot corresponding to a phase of 180° is plotted with a thick dashed red line and is marked as t_2. As it can be seen in this panel, the absolute value of the amplitude of δB_r is zero at the equatorial plane and increases rapidly as a function of latitude. Similar to the figures in Wang et al. (2018), Li, Liu, et al. (2021), and Li, Zhou, et al. (2021), only values up to 65° in latitude are plotted. Overplotted in Figure 2b are statistical measurements of the amplitudes of δB_r as a function of latitude from the THEMIS and Arase missions as shown in Figure 1, plotted here for $L = 5$, 6 and 7; these are marked with thick solid dark purple, purple, and light purple lines, respectively. For reference, in Figure 1 these three L-shells are marked with dashed lines of the same colors. Overplotted in Figure 2b are also measurements of δB_r as a function of latitude from Cluster, obtained as described in Yan et al. (2023), but also recalculated for the purposes of this study for frequencies from 0.5 to 2 mHz. The amplitudes at the same three L-shells are plotted, namely $L = 5$, 6, and 7, marked with thin solid dark blue, blue and light blue lines, respectively. We note that the amplitudes as measured by THEMIS and Arase are slightly larger than those measured by Cluster; this could be due to the different time spans of the two data sets used by Sarris et al. (2022) and Yan et al. (2023), which as discussed above are 3.5 and 19 years respectively. We also note that the model-data intercomparison presented herein is done so as to confirm that the amplitudes of the model analytic functions used in the particle tracing simulations in this study are realistic and compare reasonably well to the actual range of the measurements. Further investigation is needed, using all three data sets combined, binned by solar and geomagnetic activity levels, to provide a more thorough insight onto the amplitudes of ULF waves away from the magnetic equator as a function of activity indices, such as Kp. Figure 2c shows the theoretically expected vectors of the azimuthal component of the corresponding electric field perturbations, which are plotted as blue arrows. Similarly to Figure 2b, two snapshots are plotted, marked as t_1 and t_2, which correspond to phases 0° and 180° in the oscillation of a field line; these are plotted as solid blue and dashed blue vectors. Finally, Figure 2d shows the theoretically expected amplitudes of the electric field fluctuations, in a similar format to Figure 2b. We note that, whereas a comparison can be made between the model magnetic field oscillations and statistical measurements of the magnetic field, such statistical distributions of the amplitudes of electric field fluctuations as a function of latitude were not available at the time of this study; in view of the lack of information on the statistical behavior of electric field oscillations as a function of latitude, the electric field is obtained via their comparison with the modeled poloidal oscillations. We also note that an L-dependence in the magnetic field amplitudes can be seen at high magnetic latitudes, primarily by Cluster, which reaches higher magnetic latitudes, but also at the highest latitudes of the THEMIS-Arase data set. However, such L-dependence could not easily be extracted for the analytic formulations of the electric field; thus, no L-dependence is included in Equations 1 and 2 for the particle tracing simulations. The need for an accurate L-dependence of the wave amplitudes in future simulation efforts, supported by L-dependent electric field measurements, is further discussed below. Finally, we note that the above expressions of Equations 1 and 2 are approximately self-consistent through Faraday's law, with deviations from this assumption appearing primarily above 65° in magnetic latitude. For the demonstration purposes of this study, this is considered sufficient for the region of interest and up to the magnetic latitudes where electrons are traced in this study. We note, however, that in future studies exact and fully consistent expressions will need to be derived.

A limiting assumption of the analytic ULF waves that are used in this model is that only a poloidal mode of the field perturbations is included, and that the toroidal mode is not modeled. Furthermore, the coupling between the different modes is neglected. It is known that in the Earth's magnetosphere ULF waves are never purely poloidal or toroidal, as these wave modes are not expected to be fully decoupled in an asymmetric field. The conversion between the two modes has been investigated theoretically (see, e.g., Mann & Wright, 1995) and has been observed experimentally (Sarris et al., 2009). We note, however, that the poloidal mode is expected to have the dominant effect in radially transporting electrons, since, as presented above, it supports azimuthal electric field perturbations. This is due to the fact that the waves under consideration are long-period compared to the bounce time of particles in the assumed dipole field. Furthermore: (a) During a wave period, the compressional field alternates between adding and subtracting from the background magnetic field, but this variation is slow compared to the bounce time. (b) The compressional component is smallest at the equator and significantly larger near the ionosphere, which means that mirror points oscillate up and down slightly over a wave period. Again, the long period of the waves makes this a second-order effect.

We note that the simplified analytic model that is used herein does not pretend to be rigorous in its specification of the waves. It uses characteristic features from published (still simplified) models that have proven to be useful. This is a commonly used approach that has also been followed in, for example, Wang et al. (2018), who also considered only poloidal mode waves, and who studied the latitudinal dependence of ULF waves. As they point out, poloidal waves, through supporting poloidal/azimuthal electric fields, can accelerate particles to high energy, leading to larger radial transport and radial diffusion than toroidal mode waves; they are thus good candidates for studying resonant wave-particle interactions, whereas the effects of the compressional component are expected to be minimal compared to those of the poloidal component.

We also note that the simulations that have been presented do not include magnetospheric compression or a convection electric field but are instead based on a symmetric, purely dipolar background magnetic field model. Whereas the use of a simplified magnetospheric environment constitutes a limitation of this approach in terms of its realistic representation of radial diffusion, we note that this approach allows us to focus on the basic principles of the effects of off-equatorial ULF waves. A follow-up study should include a more realistic environment to account for all aspects contributing to radial diffusion.

4. Particle Tracing Under the Effect of 3D ULF Model Fields

In view of the current lack of analytic derivations of a pitch-angle-dependent diffusion coefficient that incorporates latitude-dependent ULF wave power, particle tracing provides a means to investigate the effects of electric and magnetic field fluctuations in diffusing and radially transporting energetic electrons. Particle tracing also enables extracting analytically parameterized formulations of diffusion coefficients, as has been demonstrated in Sarris et al. (2006) for 1D (L-dependent) diffusion coefficients. In the following, 3D guiding center particle tracing simulations are performed in a background dipole magnetic field under the effect of time-varying model ULF electric and magnetic field fluctuations that are based on the analytic models described in the previous section. In tracing an electron under the above model field fluctuations, the guiding center approximation is used to reduce the computation time. In this approximation, an electron's exact position $\boldsymbol{r}$ is replaced by the average position $\vec{\boldsymbol{R}}$ of its guiding center, where $\vec{r} = \vec{R} + \vec{\rho}$, and where $\vec{\rho}$ is the electron's instantaneous gyro-radius. The elimination of higher order terms results in the Guiding Center drift equation (Northrop, 1963), according to which the guiding center is calculated by solving numerically the following equation:

$$\frac{d\vec{R}}{dt} = \vec{v}_{E\times B} + \vec{v}_g + \vec{v}_c + \vec{v}_{//}$$

where $\vec{v}_{E\times B} = \vec{E} \times \vec{B}/B^2$ is the $E \times B$ drift of electrons in the presence of an electric field $\vec{E}$ and a magnetic field $\vec{B}$, $\vec{v}_g = \frac{\gamma\, m_e v_\perp{}^2}{q\, B\, R_E}\left(\vec{B} \times \nabla_\perp \vec{B}\right)$ is the gradient-B drift, and $\vec{v}_c = \frac{2\,\gamma\, m_e v_{//}{}^2}{q\, B\, R_E}\left(\vec{R_c} \times \vec{B}/B\right)$ is the curvature drift. In the above equations, γ is the relativistic parameter gamma, where $\gamma = \frac{1+\mathrm{KE}}{m_e}$, KE is the electron kinetic energy, m_e is the electron rest mass, R_E is one Earth Radius at the equatorial plane, q is the electron charge, c is the speed of light, $v_\perp$ and $v_{//}$ are, respectively, the perpendicular and parallel relativistic guiding center velocities of electrons.

In solving the above equations it is assumed that the electron's first adiabatic invariant, μ is conserved, where $\mu = \gamma^2 m_e\, v_\perp{}^2/2\,\mathrm{B}$, and that the electron gyro-radius, $\vec{\rho}$ is much smaller than the characteristic length scales of the system. By assuming that the particle's gyro-motion is much faster than its guiding center motion, we can treat the guiding center as the particle's average position. The guiding center approximation is particularly useful in situations where the magnetic field varies slowly compared to the gyro-radius, which is the case for Ultra-Low Frequency variations of the magnetic field that are treated herein. In such cases, we can neglect the details of the particle's cyclotron motion and focus instead on the guiding center trajectory. This simplification greatly reduces the computational complexity and time of tracing particles in magnetic fields, as it allows for much larger timesteps.

In solving the above equations, the fourth order Runge-Kutta scheme is used (see, e.g., Press, 1996). In this scheme, for given values of four variables (three variables for the electron's guiding center $\vec{R}$ and one variable for

the magnitude of the electron's parallel velocity, $v_{//}$) and their derivatives $\frac{d\vec{R}}{dt}$ and $\frac{dv_{//}}{dt}$, known at time t, the solution is advanced over a time interval dt and the incremented variables for $\vec{R}$ are returned. The derivatives $\frac{d\vec{R}}{dt}$ and $\frac{dv_{//}}{dt}$ are computed analytically at each point according to the equations by Northrop (1963), based on the values of the local electric and magnetic field.

For demonstration purposes, electrons of a single first adiabatic invariant, μ are traced in three different L. A μ-value of 1,000 MeV/G is selected for this study. The radial transport is then approximated by monitoring the change in L of traced electrons at fixed L and subsequently calculating their squared displacement, ΔL^2, over time. For linearly changing ΔL^2, the radial diffusion coefficient, D_{LL}, is defined as the rate of change of ΔL^2 in time for a large number of particles, over an interaction time $\tau >> 2\pi/f$, where f is the particle drift frequency:

$$D_{\mathrm{LL}} = \frac{\langle (\Delta L)^2 \rangle}{2\tau}$$

In the above expression, the brackets denote integration over time τ, and Δ denotes an average over a large number of particles (see also Schulz & Lanzerotti, 1974, pp. 89–92). This approach has been used in Sarris et al. (2006) to calculate the diffusion coefficient based on single particle traces in fluctuating electric and consistent magnetic fields.

As discussed above in the description of the analytic model field formulation, the ULF fluctuations are all assumed to be of azimuthal wavenumber (or mode number) $m = 1$. As discussed in Sarris et al. (2017) and shown schematically in their Figure 2, electrons that are initially in phase with ULF fluctuations of resonant frequency will move inward in L, gaining energy, whereas electrons that are out of phase with the fluctuations will lose energy, moving outward. Thus, to calculate the average squared displacement $<\Delta L^2>$ over time at a specific L, a number of electrons are distributed evenly in azimuth at that L, and the average squared displacement is calculated by taking the average of the rates of change ΔL^2 over time of all electrons. An example is shown in Figure 3a, where 36 electrons are distributed at $L = 6$ every 10° in azimuth and are traced over 10 drift periods. The instantaneous ΔL^2 for each electron is plotted in Figure 3a with solid black lines. Subsequently, the rate of change of ΔL^2 over time is calculated by performing linear fits to the instantaneous ΔL^2 for each particle; these are plotted with dashed lines in Figure 3a. Finally, $<\Delta L^2>$, the average ΔL^2 for all electrons over time at a specific L, is calculated as the average of all rates of change of ΔL^2. This is plotted with a solid thick blue line in Figure 3a and corresponds to D_{LL} at the given L and pitch angle.

The rate of change of ΔL^2 over time is then calculated by performing linear fits to the instantaneous ΔL^2; these are plotted with dashed lines in Figure 3a. Finally, $<\Delta L^2>$, the average ΔL^2 for all electrons over time at a specific L, is calculated as the average of all rates of change of ΔL^2. This is plotted with a solid thick blue line in Figure 3a and corresponds to D_{LL} at the given L and pitch angle.

A drift modulation can be seen in the solid black lines in Figure 3a that corresponds to the instantaneous ΔL^2 for each of the 36 traced electrons. This effect is due to the drift resonance between electrons at a specific L and pitch angle and the part of the broadband spectrum that has a frequency corresponding to the drift frequency of these electrons. This effect has been described in further detail in Sarris et al. (2020), where coherent electron flux oscillations in the form of periodic flux fluctuations have been demonstrated, with a drift frequency that is energy dependent. These flux oscillations have been associated in that study with the resonant interaction of electrons with ULF waves and have been identified as an indication of ongoing electron radial diffusion.

By performing similar calculations as shown in Figure 3a for electrons at different L and equatorial pitch angles, the L-dependent and pitch-angle-dependent diffusion coefficient can be derived. This is shown in Figure 3b, where the values of D_{LL} are plotted for $L = 5, 6, 7$ and for equatorial pitch angles from 30° to 80°. The calculation of D_{LL} at $L = 6$ for a pitch angle of 40° that is shown in Figure 3a with a blue line is marked with a blue dot and corresponding labels.

Together with the pitch angle-dependent diffusion coefficient, in Figure 3b we also plot the values of D_{LL} according to the analytic formulations described in Brautigam and Albert (2000) and Liu et al. (2016), for each of the three L. Following the discussion in, for example, Glauert et al. (2014) and Drozdov et al. (2021), the

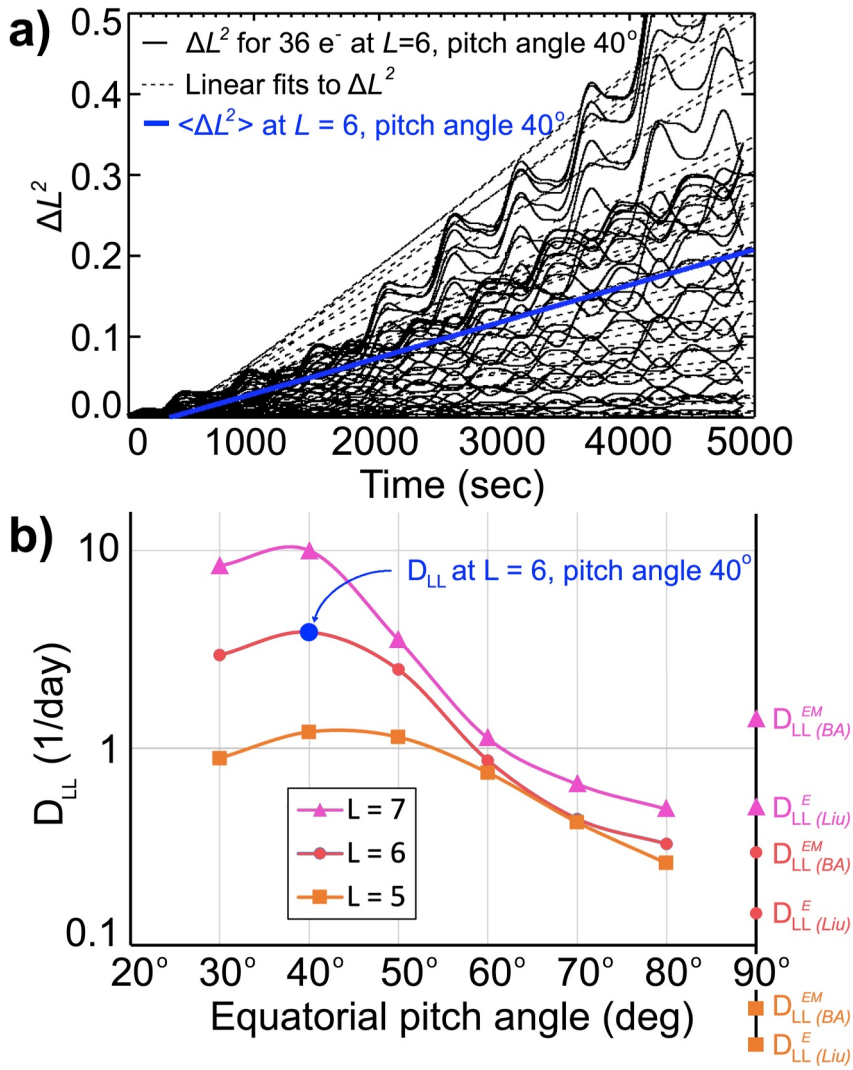

Figure 3. (a) Rates of change of the squared displacement, ΔL^2 over time, for μ = 1,000 MeV/G electrons with equatorial pitch angle of 40° at L = 6, for 36 electrons distributed evenly on the equatorial plane, every 10° in azimuth. The thick blue line shows the average squared displacement, $<\Delta L^2>$ for the 36 electrons at L = 6 and equatorial pitch angle of 40°, corresponding to D_{LL} at that L and equatorial pitch angle. (b) D_{LL} estimates for electrons of equatorial pitch angles from 30° to 80°, for L = 5, 6, and 7, calculated in a similar way as in panel (a). The D_{LL} estimation at L = 6 for equatorial pitch angle of 40° that is calculated in panel (a) as a sample is marked with a blue dot. Overplotted are estimates of D_{LL} according to Brautigam and Albert (2000) ($D_{LL}^{EM}{}_{(BA)}$) and Liu et al. (2016) ($D_{LL}^{E}{}_{(Liu)}$), for Kp = 2, at L = 5, 6, & 7, as marked.

calculations according to Brautigam and Albert (2000) correspond to the electromagnetic component of the diffusion coefficient, which is marked in Figure 3b as $D_{LL}^{EM}{}_{(BA)}$. The calculations of the diffusion coefficient according to Liu et al. (2016) correspond to the electrostatic component of the diffusion coefficient, which is marked as $D_{LL}^{E}{}_{(Liu)}$. These two diffusion coefficients are selected as representative and commonly used purely electromagnetic and purely electrostatic diffusion coefficients, and are plotted in order to provide a quantitative comparison against the values of the pitch angle-dependent diffusion coefficient. It is noted that the Brautigam and Albert (2000) diffusion coefficient is derived based on the azimuthal electric field and the compressional component of magnetic field fluctuations, and that the Liu et al. (2016) diffusion coefficient is derived based on the azimuthal electric field, whereas the model presented above is based on the azimuthal electric field and the radial component of the magnetic field. Thus, even though there are qualitative differences in the magnetic field (and thus the modes) of the waves that are considered, all three models use as input azimuthal electric field

fluctuations, which, as discussed above and also in Wang et al. (2018), have the dominant effect on radially transporting electrons in the radiation belts.

As discussed above, these estimations are applicable only to equatorial electrons, thus their values are plotted in the location along the horizontal axis corresponding to an equatorial pitch angle of 90°. Similarly to the values of the pitch angle-dependent diffusion coefficients from the traced electrons, the values of $D_{LL}{}^{EM}{}_{(BA)}$ and $D_{LL}{}^{E}{}_{(Liu)}$ are calculated at $L = 5$, 6, and 7, and are marked with the same color and shapes as the pitch-angle-dependent diffusion coefficient for each L. The values of $D_{LL}{}^{EM}{}_{(BA)}$ and $D_{LL}{}^{E}{}_{(Liu)}$ are calculated for an index of geomagnetic activity Kp = 2, corresponding to a low level of geomagnetic activity; this is further discussed below.

5. Discussion

5.1. On the Pitch Angle Dependence of the Radial Diffusion Coefficient

In Figure 3b, a clear dependence of the radial diffusion coefficient, D_{LL}, on equatorial pitch angle can be seen, with a minimum in D_{LL} observed at near-equatorial pitch angles corresponding to electrons mirroring at low magnetic latitudes, a local maximum in D_{LL} observed at pitch angles between 35° and 45° corresponding to mid latitudes and a decrease in D_{LL} observed at low pitch angles corresponding to particles mirroring at high latitudes. The values of D_{LL} for electrons with equatorial pitch angles lower than 30° have not been simulated, as there are no measurements of ULF wave fluctuations at high latitudes (above 50° magnetic latitude) to guide the model fields. It is noted that the local maximum in D_{LL} at pitch angles between 35° and 45° is due to the model of electric field fluctuations, which show a local peak at magnetic latitudes between 40° and 45° degrees; we also note that the electric field amplitudes are determined according to the theoretically expected latitudinal dependence of the electric field fluctuations of natural modes of oscillation of field lines in the magnetosphere. The determination of the latitudinal dependence of electric fields from measurements and the confirmation of the model predictions is an important study that needs to be pursued in the future.

Furthermore, in Figure 3b, a clear dependence of D_{LL} on L can also be seen. The L-dependence of D_{LL} has been discussed in several studies and is a topic of ongoing research and scientific debate, as it can affect the appearance of particle enhancements at low L and energetic electron penetration into the slot region and inner radiation belt (e.g., Mei et al., 2023; Turner et al., 2017; Zhao & Li, 2013). However, the results shown herein indicate that the expressions describing the dependence of D_{LL} on L are also a function of pitch angle, with the D_{LL} variation being more pronounced for lower pitch angles than for equatorial pitch angles. These results indicate that the L dependence of the diffusion coefficient also needs to be revisited, with more complex functions that include an equatorial pitch angle dependence, rather than the current L^n dependence that is included in most of the existing parameterizations of D_{LL} that were listed above.

In Figure 3b we also note that the D_{LL} estimations according to both Brautigam and Albert (2000) and Liu et al. (2016) are generally lower than the maximum values of the pitch angle dependent D_{LL}. At the same time, a larger spread of the D_{LL} estimations by Brautigam and Albert (2000) and Liu et al. (2016) is observed for the three D_{LL} values at $L = 5$, 6, and 7, indicating a steeper L-dependence compared to the pitch-angle-dependent D_{LL} estimations. This is because the analytic formulations of Equations 1 and 2 do not yet include an L-dependence for the oscillating field amplitudes, which according to the statistical magnetic field measurements might be significant, in particularly at higher latitudes, as indicated by Cluster measurements. Subsequent formulations in the future will need to include an L-dependence of the wave amplitudes of both the magnetic field and the electric field oscillations. It is also noted that the comparison between the pitch-angle-dependent D_{LL} estimations and the Brautigam and Albert (2000) and Liu et al. (2016) D_{LL} is performed herein for a Kp value of 2. This is because in the statistical study of Sarris et al. (2022) the wave power was obtained from 3.5 years of measurements from the THEMIS and Arase missions over the period from March 2017 to September 2020; this period corresponds to solar minimum, which indicates that the gathered statistics are strongly biased toward low Kp values. This indicates that the D_{LL} estimations can be significantly higher for higher levels of geomagnetic activity than what is plotted in Figure 3b. Subsequent studies will need to estimate the latitudinal distribution of wave amplitudes as a function of geomagnetic activity, and as a function of L and μ to obtain a corresponding activity-, pitch angle-, L- and μ-dependent diffusion coefficient.

5.2. On the Pitch Angle Dependence of Electromagnetic Versus Electrostatic Diffusion

As discussed in Fälthammar (1965), the ULF wave-driven radial diffusion coefficient can generally be separated into two different terms: the electromagnetic diffusion coefficient, which in the following will be termed D_{LL}^{EM}, and the electrostatic diffusion coefficient, which in the following will be termed D_{LL}^{E}, with the total diffusion coefficient being the sum of the two, or $D_{LL} = D_{LL}^{EM} + D_{LL}^{E}$. The first term is due to magnetic and consistent (induced) electric field fluctuations and is the part of the diffusion coefficient that is considered in the model and prescribed in the particle tracing simulations presented above. The second term consists of curl-free (electrostatic, or electric potential) fluctuations, that do not have an associated magnetic field variation. However, further to the difficulties in performing electric field measurements in space due to, for example, the spacecraft's motion in plasmas and spacecraft charging effects, differentiating between the electrostatic and electromagnetic components of the electric fields is an added complexity that remains to be resolved. This has been discussed in, for example, Perry et al. (2005) and Ozeke et al. (2012). In particular, Ozeke et al. (2012) concluded that, if the ULF fluctuating electric and magnetic fields that are causing radial diffusion are correlated through Faraday's Law, then the assumption that the two diffusion terms can be added is not straight forward, and also that one of the main assumptions that is used by Brizard and Chan (2001), namely that the fields are uncorrelated, is in violation.

Due to the above implications, the relative contribution to radial transport of D_{LL}^{EM} versus D_{LL}^{E} is a subject of debate. In Figure 3b the electromagnetic diffusion coefficient $D_{LL}^{EM}{}_{(BA)}$ appears to be higher than the electrostatic $D_{LL}^{E}{}_{(Liu)}$ for each of the three L locations. A similar conclusion has been reached by Katsavrias et al. (2022) and Thanasoula et al. (2023), who found that, during active times, D_{LL}^{EM} can be higher than D_{LL}^{E}. Contrary to that, Ozeke et al. (2014), using electric field power mapped from ground magnetometer data and compressional magnetic field power from in situ measurements, showed that the electrostatic diffusion coefficient dominates over the magnetic (or electromagnetic) diffusion coefficient. The relative contribution of the electromagnetic versus electrostatic diffusion coefficient terms has also been discussed by Tu et al. (2012) based on results from LFM MHD model runs, who, similarly to Ozeke et al. (2014), have also shown that the electrostatic diffusion term is generally much larger than the electromagnetic diffusion term. As described by these authors, since D_{LL}^{EM} is much smaller than D_{LL}^{E}, the first term can generally be neglected, providing a pragmatic solution to the problem of differentiating between the electrostatic and electromagnetic components in electric field measurements, and also validating the assumptions of Brizard and Chan (2001) and Fei et al. (2006), who separate between the two diffusion terms based on the condition of uncorrelated electric and magnetic fields. In the following, we revisit this problem and the related assumptions that are currently made in radial diffusion theory in view of the importance of off-equatorial radial diffusion.

For the field perturbations that are used in this study, it is noted that, since the model used solves for the electric and magnetic field analytically based on MHD (see, e.g., Degeling et al., 2019; Li, Liu, et al. (2021); Li, Zhou, et al., 2021; Wang et al., 2018), the electric field is prescribed consistently with the magnetic field fluctuations. The analytic functions of Equations 1 and 2 that mimic the MHD field fluctuations are similarly near-self-consistent. Thus, in the presence of a time-varying magnetic field, the electric and magnetic field variations that are prescribed in the particle tracing simulation correspond to the electromagnetic diffusion coefficient, D_{LL}^{EM}. We note, however, that, since at the equatorial plane the model fluctuations include a node for the magnetic field, but a non-zero component for the electric field, there will be a non-electromagnetic component for the electric field, which is predominant in the equatorial plane, as described below.

In Figure 4 we present the calculations of $|\vec{\nabla} \times \vec{\mathbf{E}}|$, the magnitude of the curl of the vector electric field, for a snapshot of the analytic model fields shown in Figure 2, corresponding to time t_1. In this figure, the intensity of the blue-shaded region shows the magnitude $|\vec{\nabla} \times \vec{\mathbf{E}}|$, plotted in cartesian coordinates, in units of Earth radii. Since the relative intensity of $|\vec{\nabla} \times \vec{\mathbf{E}}|$ is of interest here, a numerical scale is omitted for simplicity, and the results are discussed only qualitatively. Values from 0° to 65° in magnetic latitude are plotted, whereas values above 65° in magnetic latitude are masked as white areas.

In these calculations, a near-zero minimum can be seen in $|\vec{\nabla} \times \vec{\mathbf{E}}|$ at the equatorial plane, increasing rapidly at higher magnetic latitudes. This means that the electric field fluctuations, which according to Figure 2d are non-zero in amplitude, are almost purely electrostatic. Similarly, the diffusion coefficient is expected to be dominantly electrostatic at the magnetic equator. This also indicates that the electromagnetic field perturbations, and related

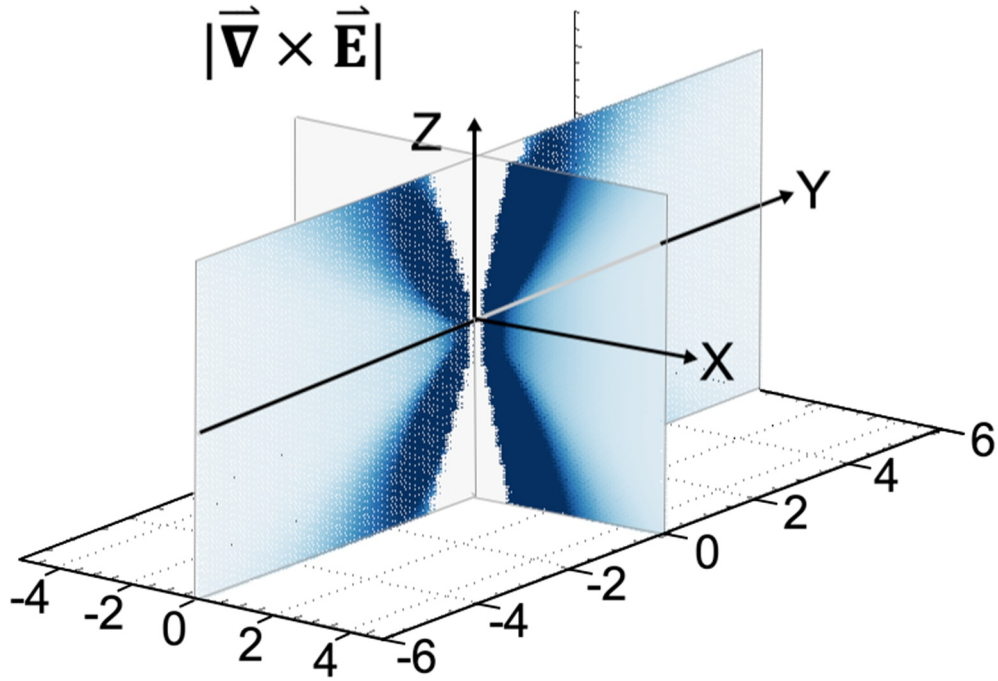

Figure 4. Calculations of the magnitude of the curl of the model electric field fluctuations for the analytic azimuthal electric field model that is presented in Figure 2, for a snapshot corresponding to time t_1 in Figure 2. Values from 0 to 65 degrees in magnetic latitude are plotted. A darker color corresponds to a higher value of the magnitude of the curl of the model electric field fluctuations.

to that, the electromagnetic diffusion coefficient, D_{LL}^{EM}, are expected to have a minimum at the equatorial plane, where, according to this model as shown in Figure 2d, the magnetic field fluctuations have a node (zero-amplitude fluctuations). This could have significant implications in the discussions on the relative contributions of D_{LL}^{EM} compared to the electrostatic diffusion coefficient, D_{LL}^{E}. For example, the conclusions by Tu et al. (2012) and Ozeke et al. (2014) on the prevalence of D_{LL}^{E} compared to the D_{LL}^{EM}, as discussed above, which were drawn based on estimates made on the equatorial plane, appear to hold true only close to the equatorial plane, where, according to the model used herein, the electric field is largely curl-free or electrostatic; however, these conclusions might not necessarily be true away from the equatorial plane. It is noted that, according to this model, there is no need to invoke separate fluctuating electromagnetic and electrostatic electric fields. Related to the above discussion, the assumptions by Brizard and Chan (2001) and Fei et al. (2006), which have been formulated for and are valid at the equatorial plane, where as shown herein the electromagnetic diffusion minimizes, might also need to be revisited away from the magnetic equator. The above discussion points to the need for detailed and accurate electric field measurements as a function of L, magnetic latitude, and geomagnetic activity, to confirm the latitudinal distribution of the electric field model that is used herein.

5.3. Implications of the Pitch Angle Dependence of Radial Diffusion

The results presented herein could have significant implications for the current understanding and quantification of radial diffusion in the radiation belts. These results emphasize the need for the advancement of 3D diffusion models that include a pitch angle dependence. Such efforts are well underway: As an example, DREAM3D (Tu et al., 2013, 2014, 2019) is a 3D diffusion model that is based on the Fokker-Planck equation (Schulz & Lanzerotti, 1974), but that includes radial, pitch angle, and momentum diffusion as well as mixed pitch angle momentum diffusion to simulate the dynamics of radiation belt electrons. Such models need to be supported by corresponding diffusion coefficients that also include an accurate pitch angle dependence. By introducing realistic diffusion coefficients into 3D diffusive models such as DREAM3D, the effects of the pitch-angle dependence of the diffusion coefficients and the related latitudinal dependence of wave power can be quantified and compared against the current models of radiation belt dynamics, that use more traditional 1D (L-dependent) diffusion coefficients.

It is noted that, in the simulations presented herein, the wave power is obtained from long-term statistics that are dominated by solar minimum conditions, corresponding to an average activity level of Kp = 2. However, during this time, a number of interplanetary coronal mass ejections and stream interaction regions were observed, which produced significantly enhanced ULF power and consequently multi-MeV electron enhancements (see, e.g., Katsavrias et al., 2022). An important next step toward introducing realistic diffusion coefficients into 3D diffusive models includes introducing a solar activity dependence by binning the power of the ULF waves also as a function of activity levels and running the corresponding simulations for different wave amplitudes.

6. Summary

The results presented herein, which show a potentially significant dependence of the radial diffusion coefficient D_{LL} on pitch angle, point toward the need for the derivation of a new, latitude-dependent diffusion coefficient. Necessary steps for the confirmation of these results include: performing statistical measurements of the electric field amplitude as a function of magnetic latitude; obtaining the latitude-dependent diffusion coefficient for different μ, across all L and for variable geomagnetic activity levels; and tracing energetic electron populations under analytic model fields for all the above cases. The end-goal is to demonstrate the level of variation of the diffusion coefficients when the pitch angle dependence and off-equatorial ULF waves are taken into account, compared to traditional radial diffusion coefficients that are dependent on only μ and L. More specifically, the following three aspects of the current formulation of the diffusion coefficient might need to be re-addressed in current models of the radiation belts: (a) a pitch-angle (PA) dependence will need to be introduced, leading from current expressions of $D_{LL}(\mu, L)$ to expressions in the form of $D_{LL}(\mu, L, \mathrm{PA})$, that take into account the latitudinal variation of ULF wave power. (b) The dependence of the diffusion coefficients on L will need to take into account the pitch angle as well, leading from expressions that are proportional to L^n to expressions in the form of $L^{n(\mathrm{PA})}$. (c) New expressions will need to be derived that differentiate between the electrostatic and electromagnetic diffusion coefficients, to account for the pitch angle dependence of the electromagnetic diffusion coefficient and its increasing importance away from the magnetic equator. Introducing a reliable pitch-angle-dependent quantification of D_{LL} in novel 3D diffusion models, such as DREAM3D, is critical to realistically simulate the long-term electron dynamics in Earth's radiation belts.

Data Availability Statement

Science data of the THEMIS satellite are publicly available and were obtained through the SPEDAS interface from the data portal maintained by the Space Sciences Laboratory of the University of California, Berkeley (http://themis.ssl.berkeley.edu/data/themis/). Science data of the ERG/Arase satellite are publicly available and were obtained through the SPEDAS interface from the ERG Science Center operated by ISAS/JAXA and ISEE/Nagoya University (https://ergsc.isee.nagoya-u.ac.jp/index.shtml.en; Miyoshi et al., 2018). The present study analyzed THEMIS state L1 data, THEMIS FGM L2 data, ERG/Arase MGF-L2 8 s spin-averaged data v01_01 (10.34515/DATA.ERG-06001), and ERG/Arase Orbit L3 v02 data (10.34515/DATA.ERG-12001).

Acknowledgments
This research was supported by NSF Grants 2140933, 2247855, 2247856 and 2247857 and by DUTH Grant KE82503. The work by W. Tu was supported by NSF Grant AGS-2247856 and NASA Grants 80NSSC21K2008, 80NSSC21K1312, 80NSSC24K1112. The publication of the article in Open Access mode was financially supported by the Hellenic Academic Libraries Link (HEAL-Link), Greece.

References

Ali, A. F., Elkington, S. R., Tu, W., Ozeke, L. G., Chan, A. A., & Friedel, R. H. W. (2015). Magnetic field power spectra and magnetic radial diffusion coefficients using CRRES magnetometer data. *Journal of Geophysical Research: Space Physics*, *120*(2), 973–995. https://doi.org/10.1002/2014JA020419

Ali, A. F., Malaspina, D. M., Elkington, S. R., Jaynes, A. N., Chan, A. A., Wygant, J., & Kletzing, C. A. (2016). Electric and magnetic radial diffusion coefficients using the Van Allen probes data. *Journal of Geophysical Research: Space Physics*, *121*(10), 9586–9607. https://doi.org/10.1002/2016JA023002

Barani, M., Tu, W., Sarris, T., Pham, K., & Redmon, R. J. (2019). Estimating the azimuthal mode structure of ULF waves based on multiple GOES satellite observations. *Journal of Geophysical Research: Space Physics*, *124*(7), 5009–5026. https://doi.org/10.1029/2019JA026927

Barker, A. B., Li, X., & Selesnick, R. S. (2005). Modeling the radiation belt electrons with radial diffusion driven by the solar wind. *Space Weather*, *3*(10). https://doi.org/10.1029/2004SW000118

Brautigam, D. H., & Albert, J. M. (2000). Radial diffusion analysis of outer radiation belt electrons during the 9 October 1990 magnetic storm. *Journal of Geophysical Research*, *105*(A1), 291–309. https://doi.org/10.1029/1999JA900344

Brautigam, D. H., Ginet, G. P., Albert, J. M., Wygant, J. R., Rowland, D. E., Ling, A., & Bass, J. (2005). CRRES electric field power spectra and radial diffusion coefficients. *Journal of Geophysical Research*, *110*(A2), A02214. https://doi.org/10.1029/2004JA010612

Brizard, A. J., & Chan, A. A. (2001). Relativistic bounce-averaged quasilinear diffusion equation for low-frequency electromagnetic fluctuations. *Physics of Plasmas*, *8*(11), 4762–4771. https://doi.org/10.1063/1.1408623

Cunningham, G. S. (2016). Radial diffusion of radiation belt particles in nondipolar magnetic fields. *Journal of Geophysical Research: Space Physics*, *121*(6), 5149–5171. https://doi.org/10.1002/2015JA021981

Degeling, A. W., Rankin, R., Wang, Y., Shi, Q., & Zong, Q.-G. (2019). Alteration of particle drift resonance dynamics near poloidal mode field line resonance structures. *Journal of Geophysical Research: Space Physics*, *124*(9), 7385–7401. https://doi.org/10.1029/2019JA026946

Dimitrakoudis, S., Mann, I. R., Balasis, G., Papadimitriou, C., Anastasiadis, A., & Daglis, I. A. (2015). Accurately specifying storm-time ULF wave radial diffusion in the radiation belts. *Geophysical Research Letters*, *42*(14), 5711–5718. https://doi.org/10.1002/2015GL064707

Drozdov, A. Y., Allison, H. J., Shprits, Y. Y., Elkington, S. R., & Aseev, N. A. (2021). A comparison of radial diffusion coefficients in 1-D and 3-D long-term radiation belt simulations. *Journal of Geophysical Research: Space Physics*, *126*(8), e2020JA028707. https://doi.org/10.1029/2020JA028707

Elkington, S. R., Chan, A. A., & Wiltberger, M. (2012). Global structure of ULF waves during the 24–26 September 1998 geomagnetic storm. In D. Summers (Ed.), *Dynamics of the Earth's radiation belts and inner magnetosphere. Geophysical monograph series* (Vol. 199, pp. 127–138). AGU. https://doi.org/10.1029/2012GM001348

Elkington, S. R., Hudson, M. K., & Chan, A. A. (2003). Resonant acceleration and diffusion of outer zone electrons in a asymmetric geomagnetic field. *Journal of Geophysical Research*, *108*(A3). https://doi.org/10.1029/2001JA009202

Escoubet, C. P., Schmidt, R., & Goldstein, M. L. (1997). Cluster-science and mission overview. *The Cluster and Phoenix Missions*, *79*(1/2), 11–32. https://doi.org/10.1023/A:1004923124586

Fälthammar, C.-G. (1965). Effects of time-dependent electric fields on geomagnetically trapped radiation. *Journal of Geophysical Research*, *70*(11), 2503–2516. https://doi.org/10.1029/JZ070i011p02503

Fälthammar, C.-G. (1968). Radial diffusion by violation of the third adiabatic invariant. In B. M. McCormac (Ed.), *Earth's particles and fields* (pp. 157–169). Reinhold.

Fälthammar, C.-G., & Walt, M. (1969). Radial motion resulting from pitch-angle scattering of trapped electrons in the distorted geomagnetic field. *Journal of Geophysical Research*, *74*(16), 4184–4186. https://doi.org/10.1029/JA074i016p04184

Fei, Y., Chan, A. A., Elkington, S. R., & Wiltberger, M. J. (2006). Radial diffusion and MHD particle simulations of relativistic electron transport by ULF waves in the September 1998 storm. *Journal of Geophysical Research*, *111*(A12), A12209. https://doi.org/10.1029/2005ja011211

Glauert, S. A., Horne, R. B., & Meredith, N. P. (2014). Simulating the Earth's radiation belts: Internal acceleration and continuous losses to the magnetopause. *Journal of Geophysical Research: Space Physics*, *119*(9), 7444–7463. https://doi.org/10.1002/2014JA020092

Hao, Y. X., Zong, Q.-G., Zhou, X.-Z., Rankin, R., Chen, X. R., Liu, Y., et al. (2017). Relativistic electron dynamics produced by azimuthally localized poloidal mode ULF waves: Boomerang-shaped pitch angle evolutions. *Geophysical Research Letters*, *44*(15), 7618–7627. https://doi.org/10.1002/2017GL074006

Huang, C.-L., Spence, H. E., Singer, H. J., & Hughes, W. J. (2010). Modeling radiation belt radial diffusion in ULF wave fields: 1. Quantifying ULF wave power at geosynchronous orbit in observations and in global MHD model. *Journal of Geophysical Research*, *115*(A6), A06215. https://doi.org/10.1029/2009JA014917

Jacobs, J. A., Kato, Y., Matsushita, S., & Troitskaya, V. A. (1964). Classification of geomagnetic micropulsations. *Journal of Geophysical Research*, *69*(1), 180–181. https://doi.org/10.1029/JZ069i001p00180

Katsavrias, C., Nasi, A., Daglis, I. A., Aminalragia-Giamini, S., Dahmen, N., Papadimitriou, C., et al. (2022). The "SafeSpace" radial diffusion coefficients database: Dependencies and application to simulations. *Annals of Geophysics*, *40*(3), 379–393. https://doi.org/10.5194/angeo-40-379-2022

Lejosne, S., Boscher, D., Maget, V., & Rolland, G. (2013). Deriving electromagnetic radial diffusion coefficients of radiation belt equatorial particles for different levels of magnetic activity based on magnetic field measurements at geostationary orbit. *Journal of Geophysical Research: Space Physics*, *118*(6), 3147–3156. https://doi.org/10.1002/jgra.50361

Li, L., Zhou, X.-Z., Omura, Y., Zong, Q.-G., Rankin, R., Chen, X.-R., et al. (2021). Drift resonance between particles and compressional toroidal ULF waves in dipole magnetic field. *Journal of Geophysical Research: Space Physics*, *126*(10), e2020JA028842. https://doi.org/10.1029/2020JA028842

Li, X.-Y., Liu, Z.-Y., Zong, Q.-G., Zhou, X.-Z., Hao, Y.-X., Pollock, C. J., et al. (2021). Off-equatorial minima effects on ULF wave-ion interaction in the dayside outer magnetosphere. *Geophysical Research Letters*, *48*(18), e2021GL095648. https://doi.org/10.1029/2021GL095648

Liu, W., Cao, J. B., Li, X., Sarris, T. E., Zong, Q.-G., Hartinger, M., et al. (2013). Poloidal ULF wave observed in the plasmasphere boundary layer. *Journal of Geophysical Research: Space Physics*, *118*(7), 4298–4307. https://doi.org/10.1002/jgra.50427

Liu, W., Tu, W., Li, X., Sarris, T., Khotyaintsev, Y., Fu, H., et al. (2016). On the calculation of electric diffusion coefficient of radiation belt electrons with in situ electric field measurements by THEMIS. *Geophysical Research Letters*, *43*(3), 1023–1030. https://doi.org/10.1002/2015GL067398

Lyon, J. G., Fedder, J. A., & Mobarry, C. M. (2004). The Lyon–Fedder–Mobarry (LFM) global MHD magnetospheric simulation code. *Journal of Atmospheric and Solar-Terrestrial Physics*, *66*(15–16), 1333–1350. https://doi.org/10.1016/j.jastp.2004.03.020

Mann, I. R., & Wright, A. N. (1995). Finite lifetimes of ideal poloidal Alfvén waves. *Journal of Geophysical Research*, *100*(A12), 23677–23686. https://doi.org/10.1029/95JA02689

Mei, Y., Li, X., Zhao, H., Sarris, T., Khoo, L., Hogan, B., et al. (2023). On the energy-dependent deep ($L < 3.5$) penetration of radiation belt electrons. *Geophysical Research Letters*, *50*(10), e2022GL101921. https://doi.org/10.1029/2022GL101921

Miyoshi, Y., Shinohara, I., Takashima, T., Asamura, K., Higashio, N., Mitani, T., et al. (2018). Geospace exploration project ERG. *Earth, Planets and Space*, *70*(1), 101. https://doi.org/10.1186/s40623-018-0862-0

Northrop, T. G. (1963). Adiabatic charged-particle motion. *Review of Geophysics*, *1*(3), 283–304. https://doi.org/10.1029/RG001i003p00283

Olifer, L., Mann, I. R., Ozeke, L. G., Rae, I. J., & Morley, S. K. (2019). On the relative strength of electric and magnetic ULF wave radial diffusion during the March 2015 geomagnetic storm. *Journal of Geophysical Research: Space Physics*, *124*(4), 2569–2587. https://doi.org/10.1029/2018JA026348

Ozeke, L. G., Mann, I. R., Murphy, K. R., Jonathan Rae, I., & Milling, D. K. (2014). Analytic expressions for ULF wave radiation belt radial diffusion coefficients. *Journal of Geophysical Research: Space Physics*, *119*(3), 1587–1605. https://doi.org/10.1002/2013JA019204

Ozeke, L. G., Mann, I. R., Murphy, K. R., Rae, I. J., & Chan, A. A. (2012). ULF wave-driven radial diffusion simulation of the outer radiation belt. In D. Summers, I. R. Mann, D. N. Baker, & M. Schulz (Eds.), *Dynamics of the Earth's radiation belts and inner magnetosphere, Geophysical Monograph Series* (Vol. 199, pp. 139–149). AGU. https://doi.org/10.1029/2012GM001332

Parker, E. N. (1960). Geomagnetic fluctuations and the form of the outer zone of the Van Allen radiation belt. *Journal of Geophysical Research*, *65*(10), 3117–3130. https://doi.org/10.1029/JZ065i010p03117

Perry, K. L., Hudson, M. K., & Elkington, S. R. (2005). Incorporating spectral characteristics of Pc5 waves into three-dimensional radiation belt modeling and the diffusion of relativistic electrons. *Journal of Geophysical Research*, *110*(A3), A03–A215. https://doi.org/10.1029/2004JA010760

Press, W. H. (1996). *Numerical recipes in Fortran 90: Volume 2, volume 2 of Fortran numerical recipes: The art of parallel scientific computing* (Vol. 2). Cambridge University Press.

Rae, I. J., Mann, I. R., Murphy, K. R., Ozeke, L. G., Milling, D. K., Chan, A. A., et al. (2012). Ground-based magnetometer determination of in situ Pc4–5 ULF electric field wave spectra as a function of solar wind speed. *Journal of Geophysical Research*, *117*(A4), A04221. https://doi.org/10.1029/2011JA017335

Roederer, J. G., & Zhang, H. (2014). Dynamics of magnetically trapped particles. In *Foundations of the physics of radiation belts and space plasmas. Astrophysics and space science library*. Springer.

Sarris, T., Li, X., & Temerin, M. (2006). Simulating radial diffusion of energetic (MeV) electrons through a model of fluctuating electric and magnetic fields. *Annals of Geophysics*, *24*(10), 2583–2598. https://doi.org/10.5194/angeo-24-2583-2006

Sarris, T. E. (2014). Estimates of the power per mode number of broadband ULF waves at geosynchronous orbit. *Journal of Geophysical Research: Space Physics*, *119*(7), 5539–5550. https://doi.org/10.1002/2013JA019238

Sarris, T. E., & Li, X. (2017). Geomagnetic activity and local time dependence of the distribution of ultra low-frequency wave power in azimuthal wavenumbers, *m*. *Annals of Geophysics*, *35*(3), 629–638. https://doi.org/10.5194/angeo-35-629-2017

Sarris, T. E., Li, X., Temerin, M., Zhao, H., Califf, S., Liu, W., & Ergun, R. (2017). On the relationship between electron flux oscillations and ULF wave-driven radial transport. *Journal of Geophysical Research: Space Physics*, *122*(9), 9306–9319. https://doi.org/10.1002/2016JA023741

Sarris, T. E., Li, X., Temerin, M., Zhao, H., Khoo, L. Y., Turner, D. L., et al. (2020). Simulations of electron flux oscillations as observed by MagEIS in response to broadband ULF waves. *Journal of Geophysical Research: Space Physics*, *125*(7), e2020JA027798. https://doi.org/10.1029/2020JA027798

Sarris, T. E., Li, X., Zhao, H., Papadakis, K., Liu, W., Tu, W., et al. (2022). Distribution of ULF wave power in magnetic latitude and local time using THEMIS and Arase measurements. *Journal of Geophysical Research: Space Physics*, *127*(10), e2022JA030469. https://doi.org/10.1029/2022JA030469

Sarris, T. E., Wright, A. N., & Li, X. (2009). Observations and analysis of Alfvén wave phase mixing in the Earth's magnetosphere. *Journal of Geophysical Research*, *114*(A3), A03218. https://doi.org/10.1029/2008JA013606

Schulz, M., & Lanzerotti, L. J. (1974). *Particle diffusion in the radiation belts*. Springer-Verlag Berlin 3364. https://doi.org/10.1007/978-3-642-65675-0

Schulz, M., & Lanzerotti, L. J. (2012). *Particle diffusion in the radiation belts* (Vol. 7). Springer Science & Business Media.

Selesnick, R., Blake, J., Kolasinski, W., & Fritz, T. (1997). A quiescent state of 3 to 8 MeV radiation belt electrons. *Geophysical Research Letters*, *24*(11), 1343–1346. https://doi.org/10.1029/97gl51407

Singer, H. J., Hughes, W. J., & Russell, C. T. (1982). Standing hydromagnetic waves observed by ISEE 1 and 2: Radial extent and harmonic. *Journal of Geophysical Research*, *87*(A5), 3519–3529. https://doi.org/10.1029/JA087iA05p03519

Takahashi, K., Glassmeier, K.-H., Angelopoulos, V., Bonnell, J., Nishimura, Y., Singer, H. J., & Russell, C. T. (2011). Multisatellite observations of a giant pulsation event. *Journal of Geophysical Research*, *116*(A11), A11223. https://doi.org/10.1029/2011JA016957

Thanasoula, K., Katsavrias, C., Nasi, A., Daglis, I., Balasis, G., & Sarris, T. (2023). The dependence of radial diffusion coefficients on solar/interplanetary drivers. *Advances in Space Research*, *71*(12), 5171–5184. ISSN: 0273-1177. https://doi.org/10.1016/j.asr.2023.02.015

Torrence, C., & Compo, G. P. (1998). A practical guide to wavelet analysis. *Bulletin of the American Meteorological Society*, *79*(1), 61–78. https://doi.org/10.1175/1520-0477(1998)079<0061:APGTWA>2.0.CO;2

Tu, W., Cunningham, G. S., Chen, Y., Henderson, M. G., Camporeale, E., & Reeves, G. D. (2013). Modeling radiation belt electron dynamics during GEM challenge intervals with the DREAM3D diffusion model. *Journal of Geophysical Research: Space Physics*, *118*(10), 6197–6211. https://doi.org/10.1002/jgra.50560

Tu, W., Cunningham, G. S., Chen, Y., Morley, S. K., Reeves, G. D., Blake, J. B., et al. (2014). Event-specific chorus wave and electron seed population models in DREAM3D using the Van Allen Probes. *Geophysical Research Letters*, *41*(5), 1359–1366. https://doi.org/10.1002/2013GL058819

Tu, W., Elkington, S. R., Li, X., Liu, W., & Bonnell, J. (2012). Quantifying radial diffusion coefficients of radiation belt electrons based on global MHD simulation and spacecraft measurements. *Journal of Geophysical Research*, *117*(A10), A10210. https://doi.org/10.1029/2012JA017901

Tu, W., Xiang, Z., & Morley, S. K. (2019). Modeling the magnetopause shadowing loss during the June 2015 dropout event. *Geophysical Research Letters*, *46*(16), 9388–9396. https://doi.org/10.1029/2019GL084419

Turner, D. L., O'Brien, T. P., Fennell, J. F., Claudepierre, S. G., Blake, J. B., Jaynes, A. N., et al. (2017). Investigating the source of near-relativistic and relativistic electrons in Earth's inner radiation belt. *Journal of Geophysical Research: Space Physics*, *122*(1), 695–710. https://doi.org/10.1002/2016JA023600

Wang, C., Rankin, R., Wang, Y., Zong, Q.-G., Zhou, X., Takahashi, K., et al. (2018). Poloidal mode wave-particle interactions inferred from Van Allen Probes and CARISMA ground-based observations. *Journal of Geophysical Research: Space Physics*, *123*(6), 4652–4667. https://doi.org/10.1029/2017JA025123

Yan, L., Liu, W., Zhang, D., Sarris, T. E., Li, X., Tong, X., & Cao, J. (2023). Cluster observation on the latitudinal distribution of magnetic Pc5 pulsations in the inner magnetosphere. *Journal of Geophysical Research: Space Physics*, *128*(10), e2023JA031789. https://doi.org/10.1029/2023JA031789

Zhang, S., Tian, A., Degeling, A. W., Shi, Q., Wang, M., Hao, Y., et al. (2019). Pc4-5 poloidal ULF wave observed in the dawnside plasmaspheric plume. *Journal of Geophysical Research: Space Physics*, *124*(12), 9986–9998. https://doi.org/10.1029/2019JA027319

Zhang, S., Tian, A., Shi, Q., Li, H., Degeling, A. W., Rae, I. J., et al. (2018). Statistical study of ULF waves in the magnetotail by THEMIS observations. *Annales Geophysicae*, *36*(5), 1335–1346. https://doi.org/10.5194/angeo-36-1335-2018

Zhao, H., & Li, X. (2013). Modeling energetic electron penetration into the slot region and inner radiation belt. *Journal of Geophysical Research: Space Physics*, *118*(11), 6936–6945. https://doi.org/10.1002/2013JA019240

Zheng, L., Chan, A. A., O'Brien, T. P., Tu, W., Cunningham, G. S., Albert, J. M., & Elkington, S. R. (2016). Effects of magnetic drift shell splitting on electron diffusion in the radiation belts. *Journal of Geophysical Research: Space Physics*, *121*(12), 11985–12000. https://doi.org/10.1002/2016JA023438